Compact Variable Stiffness Joint with Force Sensing Ability-Application to Classify Contact Surfaces

Shinya Kajikawa and Aruto Suzuki
Department of Mechanical Engineering and Intelligent Systems, Tohoku Gakuin University, Tagajo, Japan
Email: kajikawa@mail.tohoku-gakuin.ac.jp

***Abstract*—This paper describes a new compact variable stiffness joint mechanism. This mechanism is so small as to be embedded into the finger joint of a human-sized robotic hand. In the mechanism, a silicone rubber cushion, which is inserted between the motor and the output link is effectively used to adjust the joint stiffness and to sense external forces. The joint stiffness can be controlled by restricting the degree of cushion deformation with a cushion support wall (CS-wall) actuated by a pneumatic system. However, the joint stiffness is adjusted to only the lowest or highest level, because of the difficulties of achieving precise position control of the CS-wall by the pneumatic system. Conversely, the detection of external forces shows good performance. The change in the pressure inside the cushion provides information on the external forces applied to the link. We applied this function to measure the friction force between the robotic finger and the object, and attempted to determine differences in the friction force among twelve types of objects. The experimental results show that the mechanism is able to determine differences in the friction force and its oscillation between the objects. We confirmed that this ability can be used to classify objects.**

***Index Terms*—variable stiffness joint, robot finger, force estimation, estimation of contact situation**

I. INTRODUCTION

Because of the rapid growth in the aged population, there is an increasing demand for human-care robots, which would coexist in our living spaces and support our daily activities. In performing human care services such as dish washing, cooking, and healthcare, robots often must manipulate many types of objects that have different characteristics regarding their shape, hardness, smoothness, and so on. To improve the adjustability and the performance of grasping and handling variable objects, a variable stiffness joint system (VSJ) is one effective solution [1].

Many studies have investigated the VSJ mechanism. Among these studies, the human mimetic design approach, which uses artificial muscles with an antagonistic arrangement, is simple and effective [2], [3]. It can control the joint position and its stiffness independently and improves the potential for a robotic hand to accomplish dexterous manipulation.

Manuscript received April 5, 2014; revised July 12, 2014.

Pneumatic artificial muscles are often used in a VSJ because of their light weight and high output. However, they tend to oscillate and worsen the performance of position control.

Instead of pneumatic artificial muscles, two nonlinear springs were utilized in previous systems [4], [5]. These systems provide a linear relationship between co-contraction of muscles and joint stiffness, and show similar characteristics to those of biological joints. However, these systems with artificial muscles tend to be complicated and bulky.

Other effective approaches are also based on the VSJ mechanism. Their key principle is the insertion of elastic elements between the motor and the output link [6]-[8]. Morita *et al*. [6] used a leaf spring to support the output link and controlled the joint stiffness by changing the effective length of the spring. A different layout of the leaf spring was found in another mechanism [8]. This mechanism achieved fast adjustment of joint stiffness by controlling the rotational position of the leaf spring around the principal axis of the link. These mechanisms are simple and can be set up in a limited space. They also provide robotic hands with flexibility to manage unstable objects successfully.

However, robots should also be aware of the contact situation with the object to determine the way to manage the situation. Therefore, robots should have the additional ability to sense the contact state.

Kajikawa *et al*. [9] proposed a novel mechanism for a robotic finger joint that satisfies both adjustability and sensory ability by using silicone rubber cushions. In their mechanism, four hollow-shaped cushions were placed between the motor and the output link. The elastic deformation of the cushions contributed to the absorption of external forces and enabled the robotic finger to react gently. The softness of the joint was adjusted by controlling the degree of pressing the cushion against the output link. Furthermore, the changes in the pressure inside each cushion were used to estimate the direction and magnitude of external forces applied to the finger. This mechanism is useful for robots to enable them to plan dexterous motion interactively when they are in contact with the external environment.

In our study, we modified the abovementioned mechanism to reduce its size and to reduce the amount of

doi: 10.12720/joace.3.3.215-221

energy needed for stiffness adjustment. The modified joint mechanism was introduced into a prototype finger, and we examined the adjustable range of its stiffness. We also investigated differences in the surface properties by taking advantage of the ability to sense contact forces during rubbing of the object.

The ability to sense external forces and the ability to adjust joint stiffness enabled the robot to perform the desired tasks dexterously through interaction with its environment.

II. Previous Joint Mechanism

Fig. 1 shows our previous VSJ mechanism [9]. In this mechanism, two types of silicone rubber cushions, A-SRC and B-SRC, are used. A-SRC consists of four cylinder-shaped cushions,(CSCs). B-SRC is a simple doughnut-shaped cushion. Two A-SRCs are placed on each side of the output link, respectively, and one B-SRC is located between the two A-SRCs.

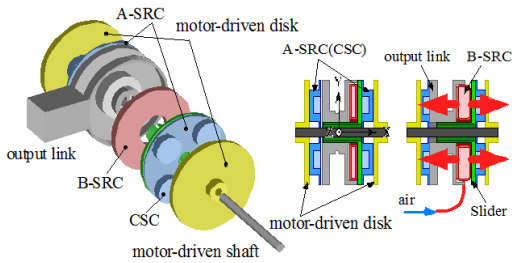

Figure. 1. Previous joint mechanism.

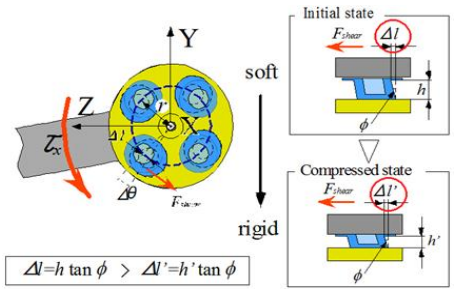

Figure. 2. Mechanism of stiffness adjustment in previous version. The reaction angle of the link, $\Delta\theta$, is proportional to Δlwhich is defined as $\Delta l = h \cdot \tan\emptyset$. Assuming the shear strain, $\tan\emptyset$, does not vary for same shearing force,F_{shear}, the height of A-SRC, h, decides the joint reaction angle, $\Delta\theta$.

Stiffness adjustment is achieved by controlling the degree of pressing A-SRC against the motor-driven disk. The mechanism of adjustment of joint stiffness is shown in Fig.1. The expansion of B-SRC results in it pressing upon A-SRC. The contact force between the CSCs and the motor-driven disk increases, and at the same time, the height of the CSC decreases. The former increases the friction force and reduces slippage of the output link on the motor-driven disk. The latter restricts the degree of the shear of the CSC (see Fig. 2). These two factors mainly contribute to realizing variable joint stiffness by controlling the pressure inside B-SRC.

In addition, the external forces around the Y-axis and the Z-axis can be estimated by using information on the pressure changes occurring inside the CSCs.

III. New Jonit Mechanism

The new joint mechanism is shown in Fig. 3. This joint has the same functions as the previous version: adjustment of joint stiffness and detection of external forces. However, in the new mechanism, these functions are accomplished more efficiently, and the joint system is more compact.

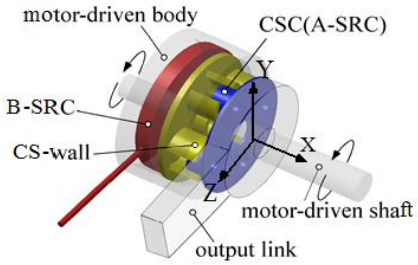

Figure. 3. Joint mechanism.

A-SRC and B-SRC are used, but they are almost half the size of those used in the previous version. A-SRC is attached to the surface of one side of the output link and is sandwiched between the output link and the motor-driven body. This cushion transmits the rotational motion from the motor to the output link by both the friction force between the surface of the CSC and the output link body and the contact force between the CSC and the cushion support wall (CS-wall).

The elastic deformations of the four CSCs absorb the external forces applied to the link. Furthermore, information on the pressure changes occurring inside each CSC is used to estimate the direction and magnitude of the external forces.

On the other hand, B-SRC has the function of adjusting the joint stiffness. This mechanism is different from that of the previous version. The expansion of B-SRC lifts the CS-wall. This wall moves to surround each CSC and applies external forces to each CSC through its contact position. The degree of the deformation of the CSC is influenced by both the positions of the applied forces and their magnitudes. That is, the joint stiffness is adjusted by controlling the height of the CS-wall.

In the previous version of the mechanism, B-SRC was placed under A-SRC and the joint stiffness was adjusted by controlling the degree of pressing A-SRC against the output link. Therefore, we must ensure that the pressure inside B-SRC is large to overcome the reaction force from A-SRC. This version of the mechanism does not seriously interfere with the movement of the CS-wall, so we do not need more energy than was needed in the previous version.

Detailed explanations of the mechanism of adjustment of joint stiffness and the detection of external forces are given in the following sections.

A. Stiffness Adjustment

The adjustment of joint stiffness can be achieved by controlling the height of the CS-wall (see Fig. 4). The external forces applied to the link generates rotational torque around the motor-driven shaft,τ_x.This torque acts on the side of the CSC as the shearing force, F_{shear},

through the CS-wall and causes deformation of the CSC. We assume that shear deformation occurs at the contact point of the CS-wall. The deformation increases in proportion to the effective height of the CSC and is obtained by the subtraction of the actual heights of the CSC, H, and the CS-wall, h. The relationship between the effective height and the deformation, Δl, is expressed as follows:

$$\Delta l = (H - h) \cdot \tan \emptyset, \tag{1}$$

where $\tan \emptyset$ means the shear strain of the CSC. Defining the shear modulus of the CSC as G, the shear strain is rewritten as

$$\tan \emptyset = \frac{F_{shear}}{A} \frac{1}{G}, \tag{2}$$

where A indicates the area of upper surface of the CSC. Considering the relationship between the rotational angle, $\Delta\theta$, and Δl, we can obtain the following model of the joint stiffness:

$$\Delta l = r\Delta\theta \tag{3}$$

$$F_{shear} = \frac{GAr}{H - h} \cdot \Delta\theta \tag{4}$$

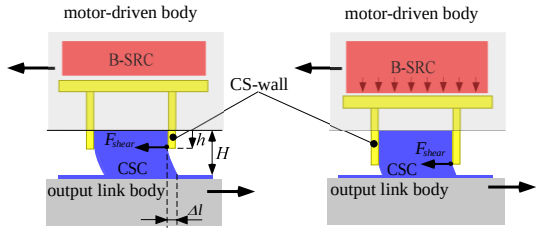

(a) low stiffness (b) high stiffness

Figure. 4. Deformation of A-SRC according to the height of CS-wall. (a) The height of the CS-wall is low; therefore, the shearing force is applied to the CSC at higher position. (b) It is difficult to deform CSC as the shear force is applied at a lower position.

where r is the distance between the centers of the CSC and the motor-driven shaft.The relationship between the external torque, τ_x, and the shearing force, F_{shear}, is given by

$$F_{shear} = \frac{\tau_x}{r} \tag{5}$$

Finally, the joint stiffness can be expressed as a function of the pressure inside B-SRC, because the height of the CS-wall is controlled by its degree of expansion.

$$K(P_b) = \frac{\tau_x}{\Delta\theta} = \frac{GAr^2}{H - h(P_b)} \tag{6}$$

B. External Force Sensing

The pressure in the CSC, P_c varies according to the compressing force caused by the external forces acting on the output link. We can estimate the direction and magnitude of the external forces by observing the change in P_c.

Fig. 5 shows the situation where CSC#3 is compressed by the external torque around the Y-axis, τ_y, and, in contrast, CSC#1 is released from it. We can see that the sum of compression forces applied to both CSC#1 and CSC#3 balances with the external force, τ_y, as below,

$$\tau_y = r(f_r^{\#1} - f_r^{\#3}), \tag{7}$$

where $f_r^{\#1}$, $f_r^{\#3}$ and r are the compressing force on CSC#1, the compressing force on CSC#3, and the distance between the center of each CSC and the center of the motor shaft,respectively.

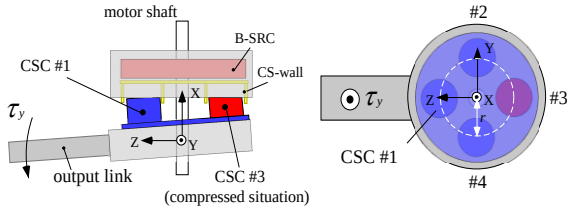

(a) top view (b) side view

Figure. 5. Compression of CSCs by an external torque around Y-axis.

If we obtain the relationship between the change in the pressure inside the CSC, ΔP_c, and the compressing force, f_r, beforehand, we can easily estimate the external force, τ_y, by measuring the pressure inside CSC#1 and CSC#3.

We can estimate the external force, τ_z, by substituting the pressure values of CSC#2 and CSC#4 for those of CSC#1 and CSC#3 in (7).

IV. Prototype Robotic Finger with the New Joint Mechanism

We fabricated a prototype finger with the proposed joint mechanism to examine fundamental performances regarding stiffness adjustment and detection of external forces. The finger and the two types of silicone rubber cushions, A-SRC and B-SRC, are shown in Fig. 6 and Fig. 7, respectively. This finger has two joints in which the proposed joint mechanism is introduced. A-SRC is inserted between the motor-driven body and the output link. The distance between them is only 3.5mm (see Fig. 6(b)). The CS-wall is pushed up or pulled down by the expansion of B-SRC and moves through the slit on the motor-driven body to surround each CSC.

Two joints are actuated by dc motors (TE-16KM-24, THINK ENGINEERING Co.,Ltd.) with a reduction gear through a worm/worm-wheel transmission.

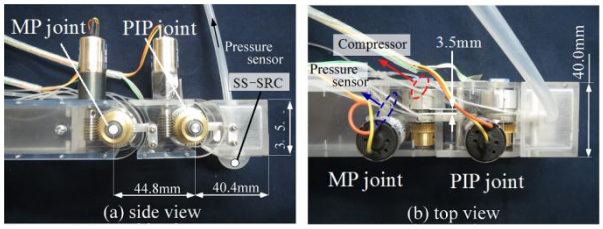

Figure. 6. Prototype robot finger.

The specifications of the motors are summarized in Table I. We used a pressure sensor, PSM-001KPGW (Fujikura Co., Ltd.) to measure the change in the pressure of each CSC. This sensor outputs a voltage signal in the range of 0.5V to 4.5V in proportion to the change in the

pressure. The specifications of this sensor are shown in Table II.

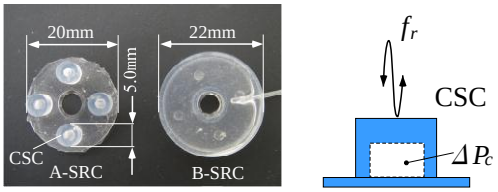

Figure. 7. Silicone rubber cushions, A-SRC and B-SRC.

TABLE I. SPECIFICATION OF ACTUATOR.

DC motor	TE-16KM-24(Think Engineering Co.,Ltd.)	
Rated speed	18,600rpm	
Rated torque	0.49mNm	
Reduction gear	MP Joint	PIP Joint
planetary gear	216:1	144:1
Wormgear&wheel	20:1	20:1

TABLE II. SPECIFICATION OF PRESSURE SENSORS.

	PSM-001KPDW (FujikuraCo.,Ltd.)	PSM-005KPGW (Fujikura Co.,Ltd.)
Pressure type	Gauge pressure	
Rated pressure	-1~1KPa	-5~5KPa
Output voltage	0. 5~4.5V	
Response time	less than 2ms	
Accuracy	±5%FS	

For the purpose of measuring the contact force, a semi-spherical silicone rubber cushion (SS-SRC) was attached to the finger-tip(see Fig. 6).We were able to estimate the contact force easily, because the pressure change in this cushion directly reflects the change in the contact force. Another pressure sensor, PSM-005KPGW (Fujikura Co., Ltd.) was used to measure the pressure inside the SS-SRC.

A. Range of Stiffness Adjustment

In Fig. 8, the experimental results of joint stiffness for two pressure settings of P_b (0 and 75KPa) are described. The positions (heights) of the CS-wall were intended to be 0.0 and 3.5mm at these pressure settings, respectively. We were not able to control the position of the CS-wall continuously by adjusting the pressure, P_b, accordingly, because the contact situation between the CS-wall and the slit on the motor-driven body was not stable and the friction force was not constant. The pneumatic control system was not able to achieve precise position or force control under this unstable condition. As a result, this joint was able to shift its stiffness only between 0.018Nm/deg and 0.086Nm/deg.

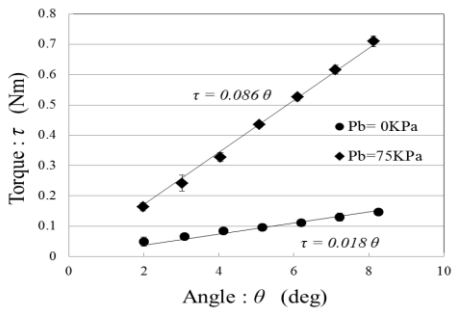

Figure. 8. Relationship between the torque and the rotational angle of the joint.

Next we discuss the maximum level of stiffness in more detail. Fig. 9 shows the theoretical values of joint stiffness based on (6). The maximum value was lower than the theoretical value. The compression of the CSC occurred along the shearing force in addition to its shear deformation. This phenomenon moves the finger link more than we expected.

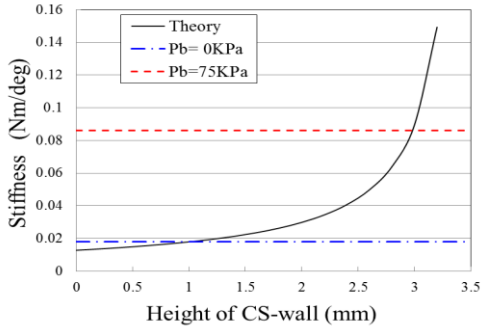

Figure. 9. Comparison of the joint stiffness.

Furthermore, the maximum level of stiffness was lower than that achieved with our previous version of the mechanism, which reached 0.29Nm/deg. The previous version utilized two A-SRCs, which were twice the size of the new A-SRC shown in Fig. 7.We believe that the size and the number of A-SRCs mainly influenced this difference observed in the maximum stiffness values.

Although the stiffness remained low, the pressure required was lower that required in the previous version of the mechanism. Pressure of 250KPa was needed to reach the maximum stiffness of 0.29Nm/deg in the previous version.

B. Force Sensing

Firstly, we investigated the relationship between the compressing force, f_r, and the pressure change inside the CSC, ΔP_c, by pushing it (see Fig.7).From this experiment, we found that the compressing force can be expressed by the following linear equation of ΔP_c.

$$f_r = 120.5\Delta P_c (R = 0.90) \quad (8)$$

Next, we attempted to estimate the external force, τ_y, by using information on the pressure inside the CSC. We pushed the finger link along the X-axis (or around the Y-axis) periodically.In this case, we obtained the following equation for the estimation by combining (7) with (8) .

$$\tau_y r = 120.5r(\Delta P_c^{\#1} - \Delta P_c^{\#3}) \quad (9)$$

In our previous version of the mechanism, A-SRC was located rotating 90deg around the motor-driven shaft from A-SRC position in the new version; therefore, the external force around the Y-axis or the Z-axis causes changes in the pressure inside all CSCs. We have to measure the change in the pressure of all CSCs and estimate the force by considering their balanced values. The new version of the mechanism simplifies this process.

Fig. 10 shows the estimation result. The estimation result coincided with the force and was highly accurate. We also can estimate τ_z by measuring the pressure inside CSC#2 and CSC#4.This method is simple but effective.

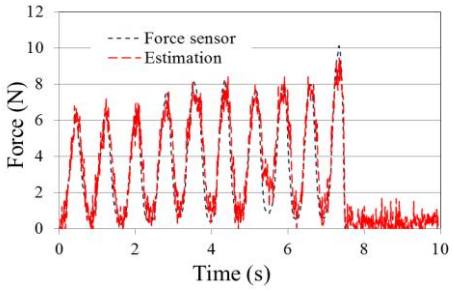

Figure. 10. Estimation result of external force around Y-axis.

In the case of the SS-SRC attached to the finger-tip, the change in the pressure, ΔP, was measured according to the compressing force, f.We obtained the following relationship by substituting the experimental data for the model obtained in our previous research[10]:

$$f = 104.96\left\{\frac{2\Delta P}{3(P_0 + \Delta P)}\right\}^{\frac{3}{4}} \quad (10)$$

where P_0 is the initial value of the pressure inside the SS-SRC.

V. Potential to Sense Texture

In this section, we describe the potential ability to sense external forces to enable the robot to interact dexterously with its external environment. Humans are able to comprehend the characteristics and condition of an object by contacting it with their fingers, and are able to manipulate it dexterously based on this perception.

The object is often rubbed to better understand its texture through the fingertip. Sensory receptors in the skin respond to the vibrations generated by stick-slip phenomena between the fingerprint and the surface of the object. Through this response, humans detect the differences in the vibration frequencies and are able to sense any unevenness of the contact surface. Although our robotic finger uses a different mechanism from that of the human finger, it shares the human finger's potential to detect vibrations as changes in external force, τ_y.

We attempted to classify a contact object by observing changes in the estimated external force, τ_y , during rubbing motion.

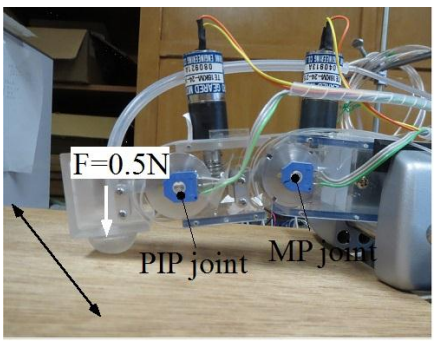

Figure. 11. Rubbing motion.

A. Experiment

The contact object was set on a stage, which was moved to the right or to the left by a linear actuator. The robotic finger was fixed by a vise on the path of the object to contact the object at its fingertip as shown in Fig. 11. We imitated robot rubbing motion by a reciprocal motion of the object. The contact object was controlled to follow a sinusoidal movement with the amplitude of $\pm$40mm at the frequency of 0.4Hz.

Conversely, the robotic finger was controlled to maintain the contact force at 0.5N based on the force estimation obtained from the pressure inside the SS-SRC. During this operation, the MP joint was controlled to maintain the lowest stiffness without expansion of B-SRC, while the PIP joint maintained its high stiffness by setting the pressure inside B-SRC to 75KPa. Under this condition, the CSCs in the MP joint became sensitive to changes in the friction force,τ_y, andthey could be used to estimate slight changes in the force.In this experiment, we prepared twelve types of objects as shown Fig. 12.

Figure. 12. Photographs of the surfaces of the object.

B. Classification

The estimated friction forces for photographic paper and a cork plate are shown in Fig. 13. As shown in these figures, the friction forces remained constant and their directions were changed periodically to synchronize with the movement of the linear stage.

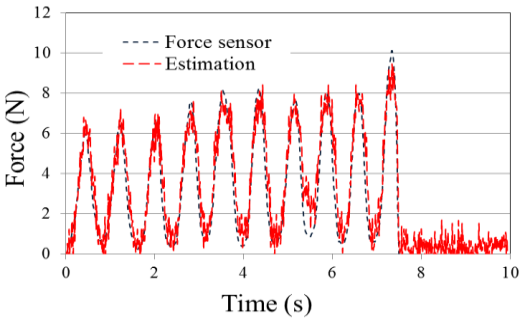

Figure. 13. Estimation result of friction force (cork and photographic paper).

We defined two types of indexes regarding the estimated τ_y to classify the contact objects.One is the

standard deviation of the estimated force (SDEF). We calculate it by using the estimated data at the period of 10sec (almost four cycles) to evaluate the magnitude of the friction force.

The other is an index that can simply express the distribution of frequency component of the oscillation of the friction force, (DFOF).

We analyzed the frequency for the estimated force of 1024points and obtained the distribution of frequency elements up to 50Hz. We calculated the sum of the frequency components of four regions, PS, from q=10 to 20Hz, 20 to 30Hz, 30 to 40Hz, and 40 to 50Hz, respectively.

In this process, we omitted any region lower than 10Hz, because it includes elements caused by the motion of the linear stage or that of the robotic finger joint. The ratio of the frequency components in each region, α_0,α_1,α_2,and α_3 , were calculated to reveal the features of the distribution of the frequency component.

$$\alpha_0 = \frac{\sum_{10}^{20} PS(q)}{\sum_{10}^{20} PS(q)} = 1, \quad \alpha_1 = \frac{\sum_{20}^{30} PS(q)}{\sum_{10}^{20} PS(q)}$$

$$\alpha_2 = \frac{\sum_{30}^{40} PS(q)}{\sum_{10}^{20} PS(q)}, \quad \alpha_3 = \frac{\sum_{40}^{50} PS(q)}{\sum_{10}^{20} PS(q)}$$

With the above parameters, we can express the distribution of the frequency component in simple bit patterns as shown below.

$$if\,\alpha_0 \geq \alpha_1\ then\ \ b_0 = 1\ \ elseif\ \ b_0 = 0$$
$$if\,\alpha_1 \geq \alpha_2\ then\ \ b_1 = 1\ \ elseif\ \ b_1 = 0$$
$$if\,\alpha_2 \geq \alpha_3\ then\ \ b_2 = 1\ \ elseif\ \ b_2 = 0.$$

The score that indicates the DFOF is given by the following equation,

$$DFOF = 2^2 \cdot b_2 + 2^1 \cdot b_1 + 2^0 \cdot b_0 \qquad (11)$$

Fig. 14 shows the distribution of the two indexes, SDEF and DFOF, for the twelve objects. This figure shows that the DFOF values are the same among the several objects. However, by adding SDEF regarding the magnitude of the friction force, all objects are isolated in this figure. Although a classification algorithm should be developed, we verified the potential to classify objects by using the features of the estimated force.

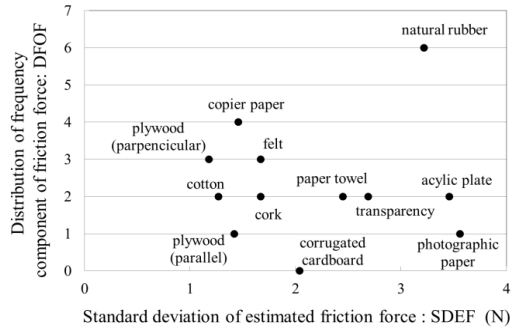

Figure. 14. Results of analysis of friction force.

VI. Conclusion

This paper described a compact mechanism that enables a robotic finger to adjust its stiffness and to sense external forces. The maximum level of stiffness was lower than that of the larger previous version of our mechanism. In addition, the stiffness could not vary continuously because of the difficulties of achieving precise control with a pneumatic system. However, the new mechanism is small and can be embedded into the robotic finger joint. We could fabricate a prototype robot finger that has two joints with new joint mechanism. Multiple arrangements of variable stiffness joints increases the adjustability of the robot to perform more difficult tasks, even if the stiffness can be set at only a low or high level.

In terms of the ability to sense external forces, the new joint mechanism showed good performance. We examined its potential ability to detect and classify the features of a contact object. The experimental results verify that the new joint mechanism is able to detect oscillations of the friction force caused by stick-slip phenomena between the fingertip and the contact surface. We expect this information to be useful in classifying objects.

Acknowledgment

This work was SUPPORTED BY 2013Adaptable and Seamless Technology Transfer Program through target-driven R&D, JST.

References

[1] R. V. Ham,T. G. Sugar, B. Vabderborght, K. W. Hollander, and D. Lefeber, "Compliant actuator designs," *IEEE Robotics and Automation Magazine*, pp. 81-94, 2009.

[2] M. Grebenstein, M. Chalon, G. Hirzinger, and R. Siegwart, "Antagonistically driven finger design for the anthropomorphic DLR hand arm system," in *Proc. IEEE-RAS Int. Conf. on Humanoid Robotics*, 2010, pp. 609-616.

[3] Shadow Robot Company Ltd. [Online]. Available: http://www.shadowrobot.com

[4] S. A. Migliore, E. A. Brown, and S. P. DeWeerth, "Biologically inspired joint stiffness control," in *Proc. IEEE Int. Conf. on Robotics and Automation*, 2005, pp. 4519-4524.

[5] K. Koganezawa, T. Inaba, and T. Nakazawa, "Stiffness and angle control of antagonistically driven joint," in *Proc. IEEE/RAS-EMBS Int. Conf. on Biomedical Robotics and Biomechanics*, 2006, pp. 1007-1013.

[6] T. Morita and S. Sugano, "Development of 4-D.O.F manipulator using mechanical impedance adjuster," in *Proc. IEEE Int. Conf. on Robotics and Automation*, 1996, pp. 2902-2907.

[7] J. Choi, S. Hong, W. Lee, S. Kang, and M. Kim, "A robot joint with variable stiffness using leaf spring," *IEEE Trans. on Robotics*, vol. 27, no. 2, pp. 229-238, 2011.

[8] S. Kajikawa, "Variable compliance mechanism for human-care robot arm," in *Proc. 33rd Annual Conf. of IEEE Industrial Electronits Society*, 2007, pp. 2738-2741.

[9] S. Kajikawa and K. Abe, "Robot finger module with multi-directional adjustable joint stiffness," *IEEE/ASME Trans. on Mechatronics*, vol. 17, no. 2, pp. 128-134, 2012.

[10] Kajikawa, "Development of robot hand aiming at nursing care services," in *Proc. IEEE Int. Conf. on Robotics and Automation*, 2009, pp. 3663-3669.

Shinya Kajikawa received the B.E.,M.E, and Ph.D. degrees in mechanical engineering from Tohoku University, Sendai, Japan, in 1991,1993, and 1996, respectively. From 1996 to 2001, he was a Research Associate in the Department of Mechanical Engineering, Miyagi National College of Technology. From 2001 to 2004,he was an Associate Professor in the Department of Intelligent Machine and Systems, Akita Prefectural University.
Since 2004, he has been with Tohoku Gakuin University, where he is currently a Professor in the Department of Mechanical Engineering and Intelligent Systems. He was a visiting professor in Technische Universitat Munchen, Germany from 2011 to 2012.
His current research interests include human-centered robotic design, dexterous robot design, human-machine interface. Prof. Kajikawa is a member of the IEEE, the Japan Society of Mechanical Engineers(JSME), the Robotics Society of Japan (RSJ), and the Society of Instrument and Control Engineers(SICE).

Aruto Suzuki received the B.E degree in mechanical engineering from Tohoku Gakuin University, Tagajo, Japan, in 2014.
His current research interest is a mechatronics design for dexterous robot system.